Available online at website: https://journal.bcrec.id/index.php/bcrec

Bulletin of Chemical Reaction Engineering & Catalysis, 21 (2) 2026, 301-311

Original Research Article

3D/1D Amine Functionalized MIL-125/TiO_2 NWs Metal-organic Framework Heterostructures for Solar Stimulated CO_2 Reduction to Green Fuels

Ji Zhang Tai[1], Wei Keen Fan[1], Hajar Alias[1*], Amnani Shamjuddin[1], Mohamad Sukri Mohamad Yusof[1], Abdul Rahman Mohamed[2], Muhammad Tahir[3]

[1]Faculty of Chemical and Energy Engineering, Universiti Teknologi Malaysia, 81310 UTM Johor Bahru, Johor, Malaysia
[2]School of Chemical Engineering, Universiti Sains Malaysia, 14300 Nibong Tebal, Penang, Malaysia
[3]Chemical and Petroleum Engineering Department, UAE University, P.O. Box 15551, Al Ain, United Arab Emirates.

Received: 1st January 2026; Revised: 25th January 2026; Accepted: 27th January 2026
Available online: 5th February 2026; Published regularly: August 2026

Abstract

The urgent need to mitigate atmospheric CO_2 and transition toward renewable energy has spurred growing interest in photocatalytic CO_2 hydrogenation. In this work, we report on the fabrication of a novel 3D/1D NH_2-MIL-125/TiO_2 nanowire (NWs) heterostructure via a straightforward mechanical assembly method, combining the excellent visible light absorption of amino-functionalized metal-organic frameworks (MOFs) with the robust charge transport properties of one-dimensional TiO_2 NWs. Structural and optical characterisations have confirmed on intimate interfacial contact and synergistic electronic interactions between the MOF and TiO_2, forming an S-scheme heterojunction which promotes an enhanced photogenerated carrier separation. Under visible light, the optimised 5 wt% NH_2-MIL-125/TiO_2 NWs composite achieved methane and CO yields of 13.98 µmol/g and 84.76 µmol/g, respectively. Notably, CH_4 production soared to 660.47 µmol/g under solar-simulated irradiation, representing a 47-fold enhancement. This significant performance boost is attributed to improved light harvesting, facilitated electron migration, and strengthened interfacial dynamics. This study provides a scalable and efficient strategy for designing hybrid MOF-semiconductor photocatalysts, offering a promising pathway for sustainable solar fuel generation.

Keywords: CO2 reduction; Metal-organic frameworks; Heterojunctions; Renewable fuels; Photocatalysis

How to Cite: Tai, J. Z., Fan, W. K., Alias, H., Shamjuddin, A., Mohamad Yusof, M. S., Mohamed, A. R., Tahir, M. (2026). 3D/1D Amine Functionalized MIL-125/TiO2 NWs Metal-organic Framework Heterostructures for Solar Stimulated CO2 Reduction to Green Fuels. *Bulletin of Chemical Reaction Engineering & Catalysis*, 21 (2), 301-311. (DOI: 10.9767/bcrec.20556)

Permalink/DOI: https://doi.org/10.9767/bcrec.20556

1. Introduction

The ever-increasing global energy demand and the extensive reliance on fossil fuels have intensified environmental concerns, particularly on the escalating levels of atmospheric carbon dioxide (CO_2) [1]. This greenhouse gas is a major contributor to global warming and climate change, posing significant risks to ecological systems and human societies [2]. In light of these challenges, converting CO_2 into valuable fuels and chemicals using sustainable energy sources has emerged as a promising strategy to mitigate carbon emissions and transition towards a circular carbon economy. Among the various CO_2 utilisation technologies, photocatalytic CO_2 reduction stands out as an environmentally benign and energy-efficient approach [3]. This process mimics natural photosynthesis by harnessing solar energy to drive the chemical transformation of CO_2 into carbon-based fuels such as methane (CH_4) and carbon monoxide (CO) [4]. The integration of solar energy not only ensures a renewable input but also offers the potential for decentralised, scalable applications [5]. However, practical implementation remains hindered by limitations

* Corresponding Author.
Email: r-hajar@utm.my (H. Alias)

in catalyst performance, particularly poor light absorption, rapid charge recombination, and insufficient selectivity toward hydrocarbon products.

To address these bottlenecks, the development of heterojunction photocatalysts has garnered significant attention. In this context, the combination of metal-organic frameworks (MOFs) and metal oxides provides an attractive pathway for enhancing photocatalytic activity [6]. NH_2-MIL-125, a titanium-based MOF functionalized with amino groups, exhibits high surface area, visible-light responsiveness, and rich coordination sites that facilitate CO_2 adsorption and activation [7]. Meanwhile, titanium dioxide (TiO_2) is a widely used support material in various fields like catalysis [8], temperature sensors [9], and anti-counterfeiting applications [10,11]. It also exhibits a reducible nature, which enables favourable electronic interactions with active metals, along with its excellent thermal and chemical stability [12-15]. Notably, TiO_2 can be synthesised in various morphologies, offering tunable physicochemical properties [16]. Baamran *et al.* [17] demonstrated that reducing the particle size of TiO_2 via the sol-gel method enhances the dispersion of Ni, leading to improved performance in phenol steam reforming. Moreover, TiO_2 can be transformed from its typical spherical form into one-dimensional (1D) nanowire architectures, which offer enhanced charge transport and surface reactivity [18]. However, the use of mechanically assembled NH_2-MIL-125/TiO_2 NWs composites with a focus on photocatalytic enhancement of CO_2 to CH_4 selectivity under solar simulation remains underexplored.

This study aims to present a novel 3D/1D NH_2-MIL-125/TiO_2 NWs composite synthesised via a straightforward mechanical assembly method. The formation of this heterostructure aims to synergistically enhance visible light harvesting, charge separation, and catalytic efficiency for solar-driven CO_2 hydrogenation. Optimal loading of NH_2-MIL-125 at 5 wt% onto TiO_2 NWs is shown to significantly improve CH_4 and CO yields under solar irradiated conditions due to intimate interactions between MOF and TiO_2 NWs. Augmented interactions between the two components ameliorated charge transfer and increased the exposed surface area to light irradiations and reactants. This work highlights a simple yet effective approach for designing MOF-based heterojunctions, providing a new pathway for the development of efficient photocatalysts for renewable fuel production.

2. Materials and Methods

2.1. Materials

Titanium(IV) dioxide (TiO_2, ≥99%), titanium isopropoxide (99.9%), and aminoterephthalic acid (H_2ATA, 99%) were purchased from Sigma Aldrich, Sodium hydroxide (NaOH) pellets (≥99%), methanol (≥95%), and N,N-dimethylformamide (DMF, ≥99%) were obtained from Emsure. Hydrochloric acid (HCl, 37%) was supplied by RCI Labscan. Distilled water was used throughout the experiments.

2.2. Catalyst Preparation

As previously reported, TiO_2 nanowires (NWs) were synthesised via a solvothermal method [18]. A 10 M NaOH solution was prepared by dissolving NaOH pellets in 20 mL of distilled water. Subsequently, 0.5 g of TiO_2 powder was added, and the mixture was stirred magnetically for one hour. The resulting white suspension was then transferred into a Teflon-lined stainless-steel autoclave and subjected to heat treatment at 200 °C for 24 hours. After the reaction, the product was washed repeatedly with distilled water and 0.1 M HCl until the pH reading approached neutral. The sample was then dried overnight at 100 °C and followed by calcination at 550 °C for five hours. The final product was denoted as TiO_2 NWs.

Consistent with previously published studies [19], the NH_2-MIL-125 was synthesised via a solvothermal method. In a typical procedure, 1.5 mmol (0.4263 g) of titanium isopropoxide and 6.6 mmol (1.0869 g) of H_2ATA were dissolved in a solvent mixture of 18 mL DMF and two mL methanol. The resulting solution was transferred into a 50 mL Teflon-lined stainless steel autoclave, sealed, and heated at 150 °C for 72 hours in a muffle furnace. After the solvothermal reaction, a yellow suspension formed, which was cooled to room temperature and then subjected to repeated washing with methanol and DMF to remove residual species that could block the framework's pores. Finally, the purified product was dried at 80 °C for 12 hours to activate the material for subsequent use.

The NH_2-MIL-125/TiO_2 NWs were synthesised using a mechanical assembly method. Initially, 0.3 g of TiO_2 NWs powder was dispersed in 30 mL of methanol (Solution A). Separately, 15 mg of NH_2-MIL-125 powders was dissolved in 10 mL of methanol (Solution B). Solution B was then added dropwise to solution A under continuous stirring. After 4 hours of stirring, the resulting mixture was dried overnight in an oven at 100 °C. The synthesised sample was designated as 5 wt% NH_2-MIL-125/TiO_2 NWs. Furthermore, the mass of NH_2-MIL-125 was adjusted to 30 mg and 45 mg to fabricate the 10 wt% and 15 wt% NH_2-MIL-125/TiO_2 NWs, respectively. Figure 1 presents the complete synthesis pathway of the NH_2-MIL-125/TiO_2 NWs catalyst.

2.3. Catalyst Characterisations

X-ray diffraction (XRD) analysis was conducted using a Bruker D8 Advance diffractometer equipped with a Cu Kα radiation source (λ = 0.154 nm) operating at 40 kV and 40 mA. Surface morphology was investigated via field emission scanning electron microscopy (FE-SEM) using a Hitachi SU8020. Elemental composition and mapping were analysed by energy-dispersive X-ray spectroscopy (EDX) on a JEOL JSM-6390LV SEM. UV–vis diffuse reflectance spectra (UV–vis DRS) of the catalysts were recorded using a SHIMADZU UV-3600Plus spectrophotometer equipped with a powder sample holder under a wavelength range from 200 to 800 nm.

2.4. Photocatalytic Activity Test

The experiment was carried out in a cylindrical stainless-steel fixed-bed photoreactor loaded with 0.1 g of pristine TiO_2 NWs. The reactor diameter and height were 6.5 cm and 7 cm, respectively, providing a total internal volume of 232.3 cm^3. A quartz window positioned above the stainless-steel chamber allowed light to enter the reactor. Before irradiation, a mixture of CO_2 and H_2O was introduced into the reactor for purging. The gases were continuously flowed through the system for 30 minutes at room temperature to ensure complete air removal. After purging, the outlet valve was closed, and the reactor pressure was adjusted to 0.3 bar. The photoreactor was then exposed to visible light for 4 hours using a 35 W Xenon (Xe) lamp with a light intensity of 20 mW cm^{-2}. A reflector was employed to focus the light onto the reactor volume. After 1 hour of irradiation, a 0.3 mL gas sample was extracted using a syringe and analysed using gas chromatography (GC). The GC system was equipped with both a thermal conductivity detector (TCD) and a flame ionisation detector (FID) to detect both CO and CH_4. The procedure was subsequently repeated using NH_2-MIL-125/TiO_2 NWs composites with varying NH_2-MIL-125 loadings (5, 10, and 15 wt%). Finally, a solar simulator with a light intensity of 100 mW cm^{-2} was then used to contrast with the 20 mW cm^{-2} visible lamp.

3. Results and Discussion

3.1. Characterisations

3.1.1. X-Ray Diffraction (XRD)

The presence of all constituent materials in the ternary NH_2-MIL-125/TiO_2 NWs composites was confirmed through XRD analysis. The successful synthesis of the NH_2-MIL-125 was evidenced by the distinct diffraction peaks observed at 2θ values of 11.5°, 16.5°, and 17.9°, corresponding to the (211), (222), and (312) crystallographic planes, respectively [20,21]. The diffraction peaks at 2θ values of 25.4°, 38.0°, 48.1°, 53.0°, 55.2°, and 62.9° correspond to the (101), (004) and (200) planes, respectively, confirming the presence of pure TiO_2 NWs. These reflections are characteristic of the anatase phase of TiO_2, indicating that the synthesised TiO_2 NWs exhibit high phase purity. This observation aligns well with previously reported data on anatase-phase TiO_2 NWs [22,23]. The close agreement between

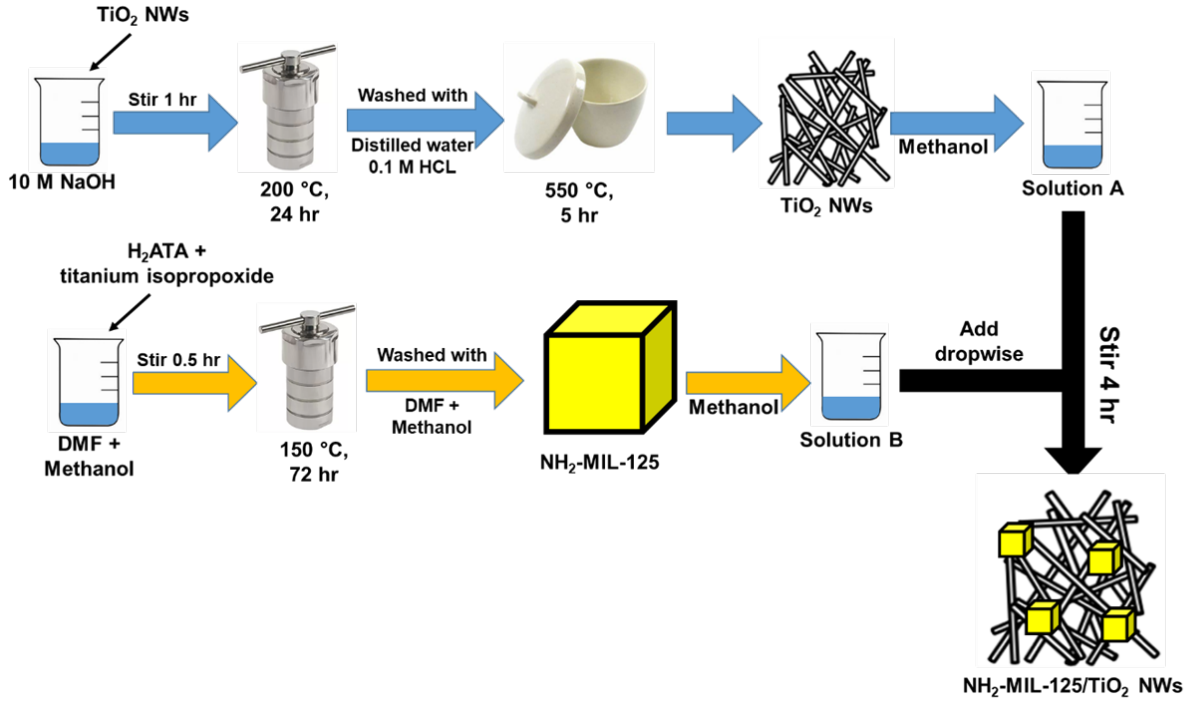

Figure 1. Synthesis procedure for the preparation of NH_2-MIL-125/TiO_2 NWs.

our XRD patterns and those in the literature further validates the successful synthesis of TiO_2 NWs in this study. These characteristic peaks were clearly present in both the pure MOF and the MOF-based composite samples, as illustrated in Figure 2. Furthermore, the XRD patterns were consistent with previously reported studies [7].

3.1.2. Morphological and structural analysis

FE-SEM was used to assess the morphological and structural characteristics of pristine TiO_2 NWs and 5% NH_2-MIL-125/TiO_2 NWs catalysts. As shown in Figure 3(a), the solvothermal synthesis produced TiO_2 with a well-defined one-dimensional (1D) nanowire morphology, which serves as a robust structural scaffold for catalyst integration. This 1D architecture facilitates high surface area exposure and provides abundant anchoring sites for MOF deposition, promoting the formation of uniformly distributed active sites while simultaneously limiting the MOF crystal growth to nanoscale dimensions. Figure 3(b) reveals that the NH_2-MIL-125 particles adopt a three-dimensional (3D) disk-like morphology with diameters ranging from 50 to 100 nm, consistent with sizes previously reported by Ikreedeegh *et al.* [19]. Although only 5 wt% NH_2-MIL-125 was incorporated, the composite exhibits a well-integrated and densely populated morphology, with MOF nanoparticles dispersed 3D across the surface and along the length of the 1D TiO_2 nanowires. This 3D dispersion is critical in maximising interfacial contact, enhancing charge transport pathways, and fully exploiting the high surface area of both components, ultimately contributing to improved catalytic efficiency in solar-driven CO_2 hydrogenation.

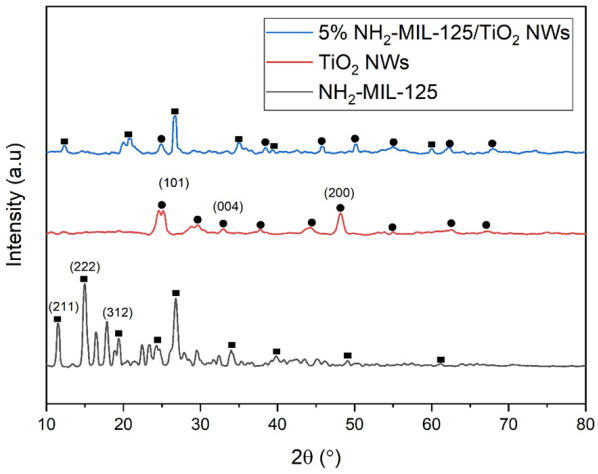

Figure 2. XRD patterns of NH_2-MIL-125, TiO_2 NWs and 5% NH_2-MIL-125/TiO_2 NWs catalysts.

3.1.3. Elemental identification and quantitative analysis

The synthesised 5% NH_2-MIL-125/TiO_2 NWs composite was further analysed using EDX for elemental identification and quantitative analysis. To ensure uniform dispersion of the NH_2-MIL-125 component, EDX spectra were acquired at multiple regions across the catalyst composite. As shown in Figure 4(a), the EDX layered image confirms a homogeneous distribution of elements throughout the sample. The elemental mapping results clearly verified the presence of Ti, O, C, and N, corresponding to the major components of the nanocomposite (Figure 4(b-d)). These findings indicate effective mixing and dispersion of both composite materials, revealing a uniform dispersion of MOF species throughout the TiO_2 NW support. Besides, these results indicate not only the uniform dispersion of MOF species throughout the TiO_2 support but also suggest an enhanced interfacial interaction between the two components. Such uniform dispersion and intimate contact are critical for facilitating efficient charge transfer, reducing electron–hole recombination, and increasing the number of accessible active sites. As reported by You *et al.*, such hierarchical 3D/1D morphologies significantly increase porosity and the active surface area, making it highly desirable for

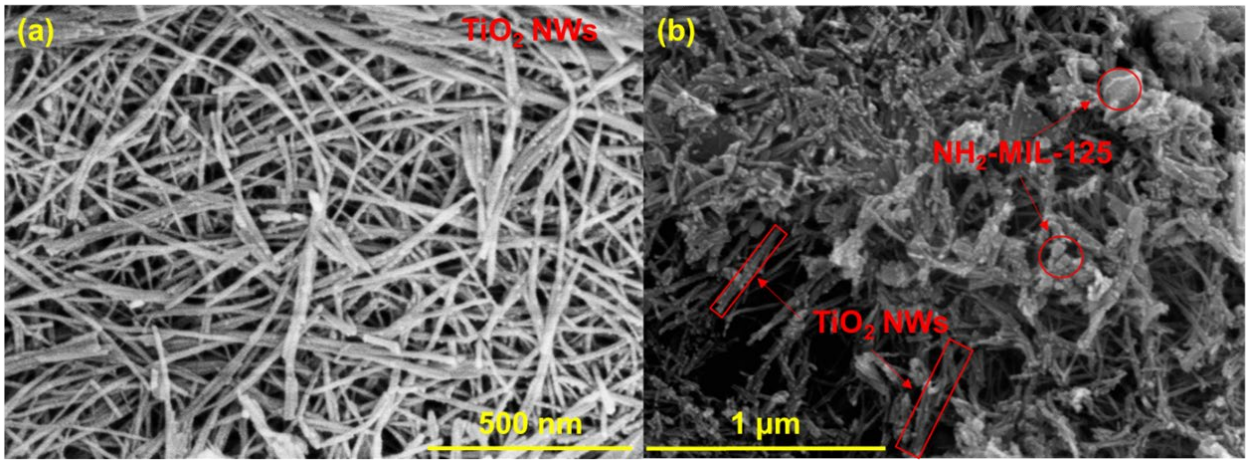

Figure 3. FE-SEM images of (a) TiO_2 NWs and (b) 5% NH_2-MIL-125/TiO_2 NWs catalysts.

enhancing intrinsic catalytic activity through improved light harvesting and charge transfer efficiency [24]. Thus, these synergistic effects ultimately contribute to improved light absorption and solar-driven conversion efficiency, thereby enhancing the overall performance of CO_2 hydrogenation to renewable fuels.

3.1.4. UV–Vis Diffuse Reflectance (UV-vis DRS)

The optical absorbance properties of NH_2-MIL-125, TiO_2 NWs and 5% NH_2-MIL-125/TiO_2 NWs catalysts were analysed using UV–vis DRS, with the spectra converted via the Kubelka–Munk function. As illustrated in Figure 5(a), pure TiO_2 NWs exhibited a narrow absorption range and low absorbance, indicating limited light-harvesting capability. The bare NH_2-MIL-125 MOF exhibited a pronounced absorption peak in the visible light region, highlighting its potential for enhanced solar energy utilisation. This strong absorption is primarily attributed to the amino functionalization of the organic linker (H_2ATA), which facilitates charge transfer from oxygen to titanium within the Ti–O clusters [25]. Upon MOF loading, the 5% NH_2-MIL-125/TiO_2 NWs displayed enhanced absorbance along with a slight red shift, suggesting improved visible-light absorption.

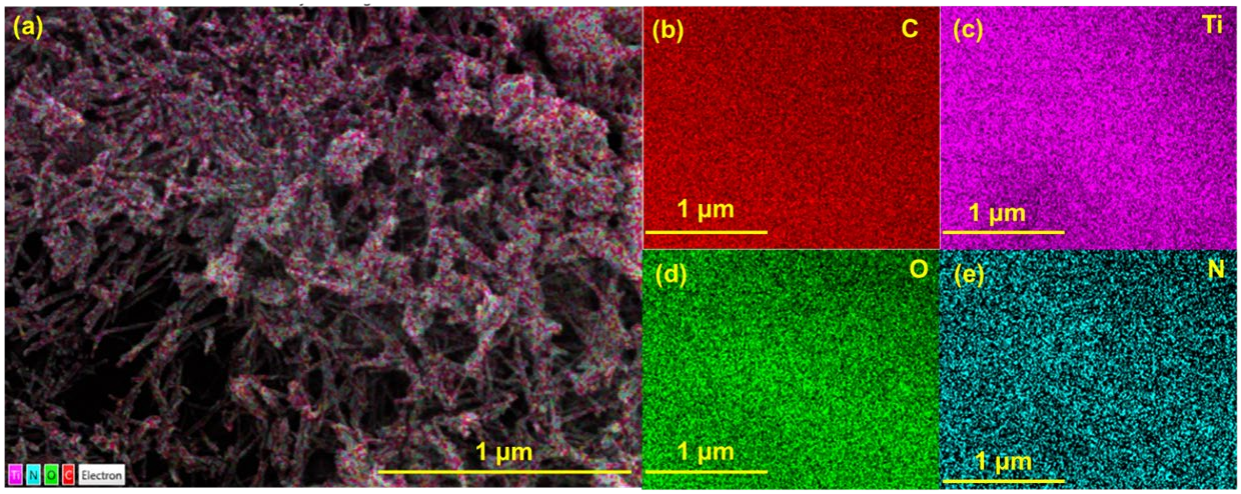

Figure 4. (a) EDX mapping and elemental distribution of (b) C, (c) Ti, (d) O and (e) N over 5% NH_2-MIL-125/TiO_2 NWs catalysts.

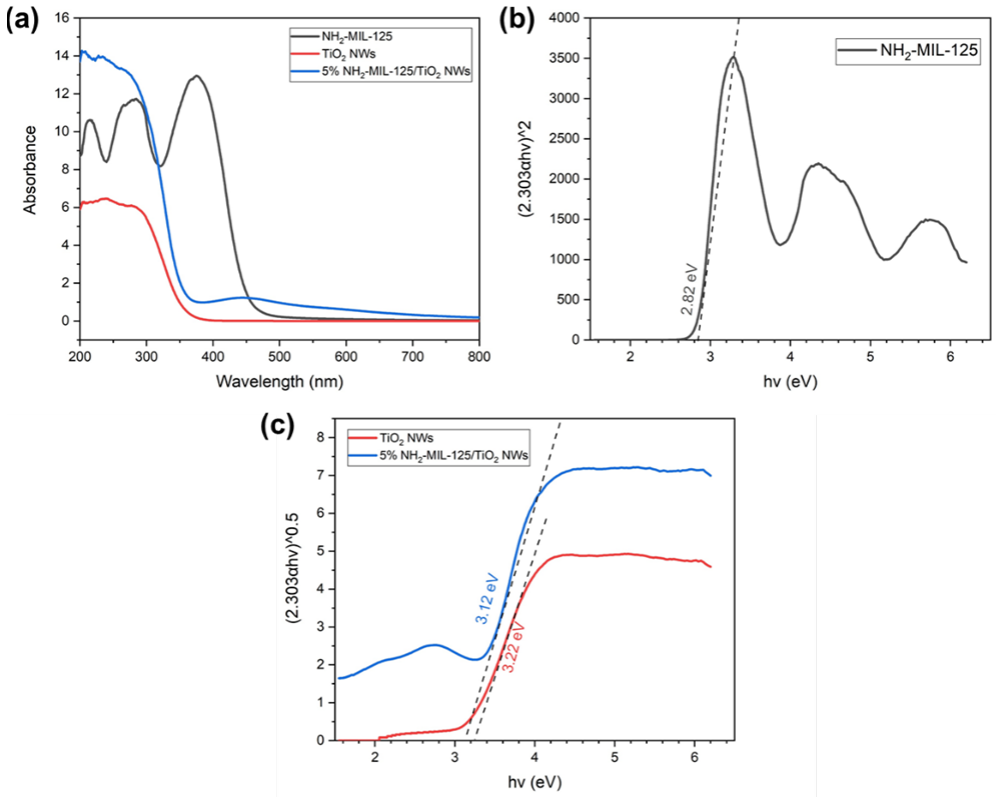

Figure 5. (a) UV–vis DRS of NH_2-MIL-125, TiO_2 NWs and 5% NH2-MIL-125/TiO_2 NWs catalysts, Tauc plot calculations of (b) NH_2-MIL-125, (c) TiO_2 NWs and 5% NH_2-MIL-125/TiO_2 NWs catalysts.

Subsequently, Tauc plots were constructed to estimate the optical band gaps (E_g) of the materials as depicted in Figure 5(b-c). The Tauc method is based on the principle that the absorption coefficient (α), as a function of photon energy (hv), can be expressed by Equation (1):

$$\alpha h\nu = B(h\nu - E_g)^m \quad (1)$$

Where B is a constant, E_g represents the band gap energy, h is Planck's constant, and ν is the frequency of the incident photon. The exponent m depends on the nature of the electronic transition: it is 1/2 for direct transitions and 2 for indirect transitions. According to the literature, NH_2-MIL-125 MOF is a direct band gap material; meanwhile, TiO_2 NWs are an indirect band gap material [26; 27]. The pure NH_2-MIL-125 MOF exhibited an E_g of 2.82 eV. Besides, the pure TiO_2 NWs exhibited an E_g of 3.22 eV. Upon MOF incorporation, the E_g of 5% NH_2-MIL-125/TiO_2 NWs decreased to 3.12 eV, suggesting narrowing of the band gap and enhanced light harvesting capability.

3.2. Photocatalytic Activity

3.2.1. Catalyst composition screening

To determine the best composite composition for photocatalytic CO_2 reduction, various amounts of NH_2-MIL-125 MOF (0, 5, 10 and 15 wt%) were incorporated into TiO_2 NWs and evaluated under visible light irradiation. As shown in Figure 6(a), the evolution of CH_4 increased progressively with irradiation time across all composite variations. In contrast, CO production exhibited an increasing trend during the first 3 hours, followed by a slight decline in the final hour of irradiation (Figure 6(b)). Pristine TiO_2 was subjected as a control sample to demonstrate that the incorporation of NH_2-MIL-125 MOF improves the production of CH_4. Notably, the composite containing 5 wt% NH_2-MIL-125 MOF exhibited the highest photocatalytic efficiency after 4 hours of irradiation, achieving CH_4 and CO production rates of 13.98 and 84.76 µmol/g, respectively. It is also the only composite that showed the yield of CH_4 and CO in the first hour of irradiation. Compared to pristine TiO_2 NWs, these values correspond to enhancements of approximately 7% for CH_4 and 230% for CO, confirming the beneficial role of MOF in boosting photocatalytic performance. As evidenced by the UV–vis DRS absorbance spectrum, the composite exhibited a noticeable red shift toward the visible light region, indicating enhanced light-harvesting capability and improved photocatalytic activity. The positive effect of this reduction was further supported by characterisation results, where the 5% NH_2-MIL-125/TiO_2 NWs composite demonstrated superior optoelectronic properties with a narrowing of E_g compared to the TiO_2 NWs counterpart. These enhancements included greater visible light absorption and more efficient electron–hole pair separation, both of which contribute to improved photocatalytic performance.

3.2.2. Light source screening

Different light sources were employed in the photocatalytic CO_2 reduction experiments to evaluate the performance of the composites under solar-driven conditions. As illustrated in Figure 7(a), irradiation using a solar simulator led to a notable enhancement in the production of both CH_4 and CO compared to visible light irradiation. There is no CH_4 and CO production under dark conditions. The improvement was particularly significant for CH_4 production, which also showed increased selectivity under solar simulator conditions. After 4 hours of irradiation, CH_4 and

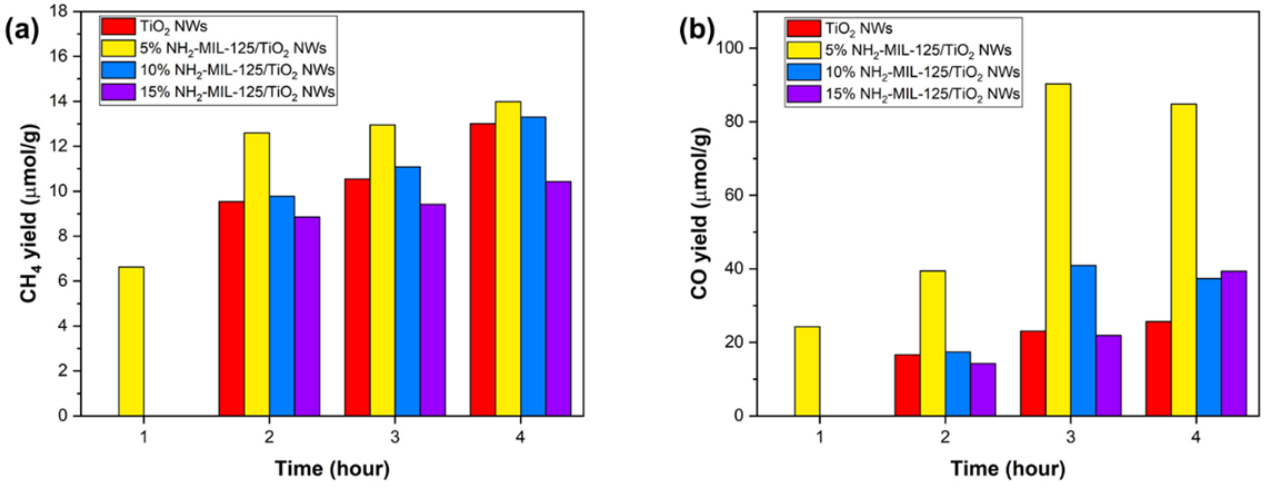

Figure 6. Effect of NH_2-MIL-125 loadings on (a) CH_4 yield and (b) CO yield. (Operating conditions: Room temperature, pressure of 0.3 bar, catalyst weight of 0.1 g and visible light irradiation of 20 mW.cm^{-2}).

CO yields under the solar simulator reached 660.47 and 104.57 µmol/g, representing 47.23-fold and 1.23-fold increases, respectively, compared to visible light (Figure 7(b-c)).

The solar simulator operated at an intensity of 100 mW/cm², whereas the visible light source was limited to 20 mW/cm². Therefore, the generation of CH_4 was favoured under solar simulator irradiation due to its higher light intensity and the presence of the whole light spectrum, which encompasses ultraviolet (UV), visible, and infrared (IR) wavelengths. The reported enhancement under solar simulator reflects a system-level increase in total energy input rather than a normalised improvement in intrinsic quantum efficiency. Furthermore, the enhanced photon energy under these conditions significantly boost electrons generation within the catalyst composites, thereby facilitating the CO_2 to CH_4 conversion reaction.

Control experiments confirmed that the evolved CH_4 originated from CO_2 reduction rather than catalyst degradation. No CH_4 or CO was detected when the reactor was fed with only H_2O under irradiation, nor were any products observed in the absence of the photocatalyst. This confirms that product formation was driven solely by the photocatalytic hydrogenation of CO_2.

3.3. Mechanism of Solar-Driven CO_2 Reduction

The direction of charge transfers within the composite was determined by using the E_g of TiO_2 NWs to calculate the valence band edge (E_{VB}) and conduction band edge (E_{CB}) positions based on the well-established empirical Equations (2) and (3):

$$E_{CB} = X - E^e - 0.5E_g \quad (2)$$

$$E_{VB} = E_{CB} + E_g \quad (3)$$

Where E^e is the energy of free electrons on the hydrogen scale (4.5 eV), E_g is the band gap energy (3.22 eV for TiO_2 NWs), and X is the absolute electronegativity or Mulliken's electronegativity of the semiconductor (5.81 eV for TiO_2 NWs).

By using equation (2), the E_{CB} of TiO_2 NWs was calculated to be -0.30 eV, while the E_{VB} was determined as 2.92 eV using equation (3). These results are consistent with previous studies [28], which reported similar E_{CB} and E_{VB} values for

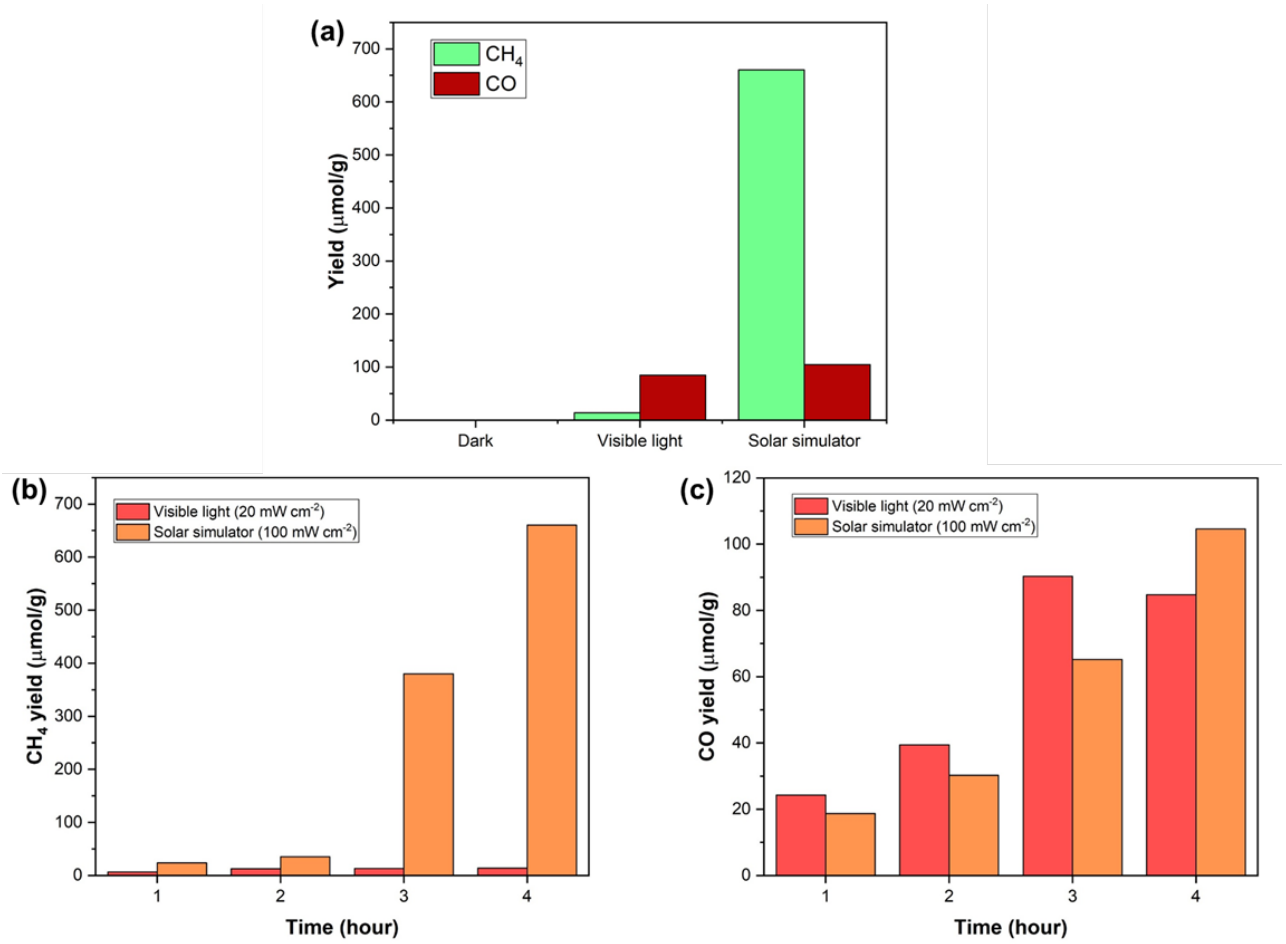

Figure 7. (a) Performance of CO_2 hydrogenation at 4 hr under dark, visible light and solar simulator irradiations. Effect of different light sources on (b) CH_4 yield and (c) CO yield at different times. (Operating conditions: Room temperature, pressure of 0.3 bar, catalyst weight of 0.1 g of 5% NH_2-MIL-125/TiO_2 NWs).

TiO_2 NWs at -0.37 eV and 2.72 eV, respectively. In contrast, the NH_2-MIL-125 MOF has reported the lowest unoccupied molecular orbital (LUMO) and the highest occupied molecular orbital (HOMO) positions of -0.82 eV and 1.85 eV, respectively, as noted in the literature [29]. Given that the experimentally observed band gap of the MOF in this study (E_g = 2.82 eV) closely matches the reported data (E_g = 2.67 eV) [29], these literature-based band positions were adopted to construct the band structure alignment.

Based on the band structure alignment of NH_2-MIL-125 MOF and TiO_2 NWs, as illustrated in Figure 8, the experimental results represent a strong deviation from a conventional Type-II heterojunction, instead suggesting the formation of an S-scheme charge transfer mechanism. Under light irradiation, both NH_2-MIL-125 MOF and TiO_2 NWs were photoexcited, generating electron–hole pairs. The photogenerated electrons in the conduction band (CB) of TiO_2 NWs recombine with the residual holes in the HOMO of NH_2-MIL-125 MOF, forming an S-scheme heterojunction. This recombination pathway preserves the charge carriers with the strongest redox potentials. Although a Type-II heterojunction is theoretically possible based on potential gradients, it would result in electrons accumulating at the TiO_2 NWs CB (–0.30 eV). This potential is thermodynamically insufficient for the CO_2 to CO conversion, which requires a reduction potential (E_p) of –0.52 eV. For the redox reaction to occur, the LUMO or CB of the photocatalyst must be more negative than its reduction potential. In contrast, the S-scheme mechanism retains electrons in the NH_2-MIL-125 MOF LUMO (–0.82 eV), which provides a significant thermodynamic driving force for the reduction reaction. Thus, the band alignment and the specific reduction potential requirements jointly confirm the operation of an S-scheme mechanism.

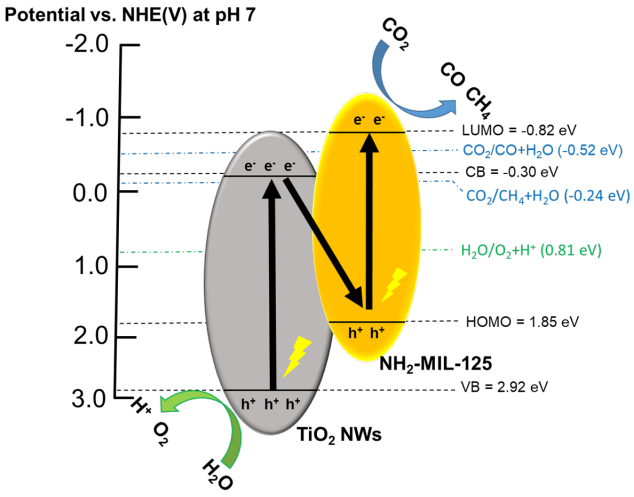

Figure 8. Schematic presentation for photocatalytic CO_2 reduction and the formation of S-scheme heterojunction over the 5% NH_2-MIL-125/TiO_2 NWs catalyst under visible light and solar simulator.

The composite's architecture plays a pivotal role in enabling this mechanism. The 1D TiO_2 NWs provide directional electron transport pathways and reduce charge scattering, while also offering high surface area for MOF anchoring. Simultaneously, the 3D dispersion of disk-like NH_2-MIL-125 MOF particles ensures intimate contact with the TiO_2 surface, maximising interfacial junctions and promoting efficient charge migration across the heterojunction. This synergistic 1D/3D structure enhances light harvesting, accelerates charge transfer, and suppresses recombination, all of which contribute to higher photocatalytic efficiency.

During the solar-driven CO_2 reduction process, the oxidation reaction occurs at the VB of the TiO_2 NWs, where photogenerated holes are consumed to produce protons and molecular oxygen, as shown in Equation (4). Simultaneously, as illustrated in Equations (5) and (6), the photogenerated electrons participate in the reduction of CO_2, where the formation of CO and CH_4 involves the transfer of two and eight electrons, respectively. The product selectivity is heavily influenced by the availability of photogenerated electrons, as indicated in Figure 7(b-c). Under visible light irradiation, the lower light intensity results in a lower generation rate of photoexcited electrons. Consequently, CO becomes the dominant product because its formation requires only two electrons, making it kinetically more favourable under electron-limited conditions. In contrast, the solar simulator provides significantly higher incident energy, generating a much higher density of electrons on the catalyst surface. This abundance of charge carriers facilitates the more complex, multi-electron reduction of CO_2 to CH_4 (eight electrons). The preservation of strong redox potentials within this S-scheme heterojunction is crucial for driving both half-reactions efficiently, and the composite's tailored nanostructure is instrumental in supporting this functionality.

$$2H_2O + 4h^+ \rightarrow O_2 + 4H^+ \quad E_P = +0.81\ eV \qquad (4)$$
$$CO_2 + 2H^+ + 2e^- \rightarrow CO + H_2O \quad E_P = -0.52\ eV \qquad (5)$$
$$CO_2 + 8H^+ + 8e^- \rightarrow CH_4 + 2H_2O \quad E_P = -0.24\ eV \qquad (6)$$

4. Conclusion

In this study, NH_2-MIL-125/TiO_2 NWs composites were successfully synthesised via a combination of solvothermal and mechanical assembly methods and evaluated for solar-driven photocatalytic CO_2 reduction. Structural, morphological, and optical characterisations confirmed the successful integration of the MOF

and TiO_2 NWs, with enhanced light absorption, reduced band gap, and well-dispersed active components. Photocatalytic testing under visible light revealed that the 5% NH_2-MIL-125/TiO_2 NWs composite exhibited the highest activity, achieving CH_4 and CO yields of 13.98 µmol/g and 84.76 µmol/g, respectively. Remarkably, under solar-simulated irradiation, CH_4 production surged to 660.47 µmol/g, demonstrating a 47-fold improvement compared to visible light conditions. This substantial enhancement is attributed to synergistic effects between the MOF and TiO_2 NWs, including improved light harvesting with a formed S-scheme heterojunction, efficient charge separation, and the one-dimensional nanowire morphology facilitating charge transport. This approach not only broadens the light absorption spectrum but also optimises interfacial charge dynamics, offering a promising strategy for efficient solar to renewable fuel conversion in CO_2 hydrogenation systems. Future investigations will prioritise a comprehensive evaluation of the long-term stability and recyclability of the amine-functionalized MIL-125/TiO2 NWs. These longitudinal studies, which were constrained in the current work by temporary equipment unavailability, are essential to fully establish the industrial viability of the proposed photocatalyst.

Acknowledgment

The authors would like to acknowledge the financial support from the Ministry of Higher Education under the Fundamental Research Grant Scheme (FRGS) (FRGS/1/2024/TK08/UTM/02/3) and Malaysia Research University Network Grant (MRUN) (R.J130000.7351.4L952).

CRedit Author Statement

Author Contributions: J.Z. Tai: Conceptualization, Methodology, Formal Analysis, Data Curation, Writting Draft Preparation. W. K. Fan: Conceptualization, Methodology, Formal Analysis, Data Curation, Writting Draft Preparation, Supervision. H. Alias: Conceptualization, Methodology, Investigation, Resources, Data Curation, Writing, Review and Editing, Supervision, Funding acquisition. A. Shamjuddin: Supervision, Funding acquisition. M. S. M. Yusof: Supervision, Funding acquisition. M. Tahir: Funding acquisition. A. R. Mohamed: Funding acquisition. All authors have read and agreed to the published version of the manuscript.

References

[1] Absalan, Y., Gholizadeh, M., Kim, E.-B., Ameen, S., Wang, Y., Wang, Y., He, H. (2024). Recent progress on organic metal compound/MOF hybrids: From controllable synthesis to potential catalytic applications. *Coordination Chemistry Reviews, 515*, 215972. DOI: 10.1016/j.ccr.2024.215972

[2] Tai, J. Z., Alias, H., Shamjuddin, A., Yusof, M.S. M., Fan, W.K. (2025). Fundamentals and advances in photothermal CO_2 hydrogenation to renewable fuels over MOF-hybrid catalysts: A review. *Journal of Environmental Chemical Engineering, 13*(3), 116291. DOI: 10.1016/j.jece.2025.116291

[3] Zhou, J., Zhao, X., Huang, L., Zhang, Y., Zhou, X., Fan, Y., Mo, S., Sun, Y., Xie, Q.,Ye, D. (2025). A C-modified engineering strategy of porous In_2O_3 catalysts for point-concentrated solar-driven photothermal CO_2 hydrogenation. *Separation and Purification Technology, 355*, 129672. DOI: 10.1016/j.seppur.2024.129672

[4] Wang, Z., Wang, Y., Li, W., Liu, S., Zhang, L., Yang, J., Feng, C., Chong, R., Zhou, Y. (2025). Integrating carbon quantum dots with oxygen vacancy modified nickel-based metal organic frameworks for photocatalytic CO_2 reduction to CH_4 with approximately 100 % selectivity. *Journal of Colloid and Interface Science, 678*, 689-702. DOI: 10.1016/j.jcis.2024.08.214

[5] Saadh, M.J., Mustafa, M.A., Altalbawy, F.M.A., Ballal, S., Prasad, G.V.S., Al-saray, M.J., Abbas, J.K., Al-Maliky, M.A., Mohammed, S.K., Alam, M.M., Elawady, A. (2025). Integration TiO_2 nanosheets into defect engineered Zr-based MOF for highly selective and efficient photocatalytic conversion of CO_2 to ethane. *Journal of Molecular Structure, 1325*, 140830. DOI: 10.1016/j.molstruc.2024.140830

[6] Abazari, R., Sanati, S., Fan, W.K., Tahir, M., Nayak, S., Parida, K., El-Shahat, M., Abdelhameed, R.M., Nesterov, D.S., Kirillov, A.M., Qian, J. (2025). Design and engineering of MOF/LDH hybrid nanocomposites and LDHs derived from MOF templates for electrochemical energy conversion/storage and environmental remediation: Mechanism and future perspectives. *Coordination Chemistry Reviews, 523*, 216256. DOI: 10.1016/j.ccr.2024.216256

[7] Yan, R., Zhi, S., Hao, M., Liu, Y., Wang, H., Zhou, S., Jiang, K., Wu, D. (2025). NH_2-MIL-125(Ti)/TiO_2 heterojunction with non-disturbed dual reactive centers for synchronous photocatalytic removal of Cr(VI) and organic dyes. *Chemosphere, 370*, 143935. DOI: 10.1016/j.chemosphere.2024.143935

[8] Hossen, M.A., Ikreedeegh, R.R., Aziz, A.A., Zerga, A.Y., Tahir, M. (2024). Carbon-based nanomaterials (CNMs) modified TiO_2 nanotubes (TNTs) photo-driven catalysts for sustainable energy and environmental applications: A comprehensive review. *Journal of Environmental Chemical Engineering, 12*. DOI: 10.1016/j.jece.2024.114088

[9] He, Y., Zhan, Y., Cun, Y., Bai, X., Zi, Y., Xu, Z., Haider, A.A., Qiu, J., Song, Z., Zhou, D., Yang, Y., Li, Y., Huang, A., Yang, Z. (2022). Designing and temperature sensing characteristics of upconversion luminescence core-shell structures with negative and positive thermal expansion. *Ceramics International, 48*(17), 24649-24655. DOI: 10.1016/j.ceramint.2022.05.110

[10] Fu, S., Huang, A., Zhao, H., Zi, Y., Bai, X., Gao, Z., Haider, A.A., Liu, Y., Cun, Y., Song, Z., Qiu, J., Tatiana, C., Yang, Z. (2025). Kinetics-Tunable Photochromism and Dual-Mode Luminescence Modulation in $BaTiO_3$-Based Phosphors for Dynamic Anti-Counterfeiting Application. *Advanced Optical Materials, 13*(8), 2402707. DOI: 10.1002/adom.202402707

[11] Haider, A.A., Cun, Y., Bai, X., Xu, Z., Zi, Y., Qiu, J., Song, Z., Huang, A., Yang, Z. (2022). Anti-counterfeiting applications by photochromism induced modulation of reversible upconversion luminescence in TiO_2:Yb^{3+},Er^{3+} ceramic. *Journal of Materials Chemistry C, 10*(16), 6243-6251. DOI: 10.1039/D2TC00859A

[12] Abbas, T., Tahir, M., Saidina Amin, N.A. (2018). Enhanced metal–support interaction in $Ni/Co_3O_4/TiO_2$ nanorods toward stable and dynamic hydrogen production from phenol steam reforming. *Industrial & Engineering Chemistry Research, 58*(2), 517-530. DOI: 10.1021/acs.iecr.8b03542

[13] Etacheri, V., Di Valentin, C., Schneider, J., Bahnemann, D., Pillai, S.C. (2015). Visible-light activation of TiO_2 photocatalysts: Advances in theory and experiments. *Journal of Photochemistry and Photobiology C: Photochemistry Reviews, 25*, 1-29. DOI: 10.1016/j.jphotochemrev.2015.08.003

[14] Jaksani, B., Chauhan, R., Kshirsagar, S.D., Rana, A., Pal, U., Singh, A.K. (2024). A MOF-derived CuO/TiO_2 photocatalyst for methanol production from CO_2 reduction in an AI-assisted continuous flow reactor. *Chemical Communications, 60*(96), 14212-14215. DOI: 10.1039/d4cc05008h

[15] Fan, W.K., Tahir, M., Alias, H. (2024). Visible light promoted low temperature photothermal CO_2 methanation over morphologically engineered Ni/TiO_2 NWs catalyst. *Materials Today: Proceedings*. DOI: 10.1016/j.matpr.2023.05.665

[16] Fan, W.K., Tahir, M., Alias, H.,Mohamed, A.R. (2024). Well-Designed morphology regulated ZIF-67 derived 0D/1D Co_3O_4@TiO_2 NWs integrated with in-situ grown Ni/Co-Active metals for Low-Temperature driven CO_2 methanation. *Fuel, 357*, 130024. DOI: 10.1016/j.fuel.2023.130024

[17] Baamran, K.S., Tahir, M., Mohamed, M., Khoja, A.H. (2020). Effect of support size for stimulating hydrogen production in phenol steam reforming using Ni-embedded TiO_2 nanocatalyst. *Journal of Environmental Chemical Engineering, 8*(1), 103604. DOI: 10.1016/j.jece.2019.103604

[18] Fan, W.K., Tahir, M. (2022). Investigating the product distribution behaviour of CO_2 methanation through thermodynamic optimized experimental approach using micro/nano structured titania catalyst. *Energy Conversion and Management, 254*. DOI: 10.1016/j.enconman.2022.115240

[19] Ikreedeegh, R.R., Tahir, M. (2021). Indirect Z-scheme heterojunction of NH_2-MIL-125(Ti) MOF/g-C_3N_4 nanocomposite with RGO solid electron mediator for efficient photocatalytic CO_2 reduction to CO and CH_4. *Journal of Environmental Chemical Engineering, 9*(4), 105600. DOI: 10.1016/j.jece.2021.105600

[20] Han, X., Yang, X., Liu, G., Li, Z., Shao, L. (2019). Boosting visible light photocatalytic activity via impregnation-induced RhB-sensitized MIL-125 (Ti). *Chemical Engineering Research and Design, 143*, 90-99. DOI: 10.1039/D2TC00859A

[21] Rahmani, A., Emrooz, H.B.M., Abedi, S., Morsali, A. (2018). Synthesis and characterization of CdS/MIL-125 (Ti) as a photocatalyst for water splitting. *Materials Science in Semiconductor Processing, 80*, 44-51. DOI: 10.1016/j.mssp.2018.02.013

[22] Kang, Y., Jiao, S., Wang, B., Lv, X., Wang, W., Yin, W., Zhang, Z., Zhang, Q., Tan, Y., Pang, G. (2020). PVDF-modified TiO_2 nanowires membrane with underliquid dual superlyophobic property for switchable separation of oil–water emulsions. *ACS Applied Materials & Interfaces, 12*(36), 40925-40936. DOI: 10.1021/acsami.0c11266

[23] Tshabalala, Z.P., Mokoena, T.P., Jozela, M., Tshilongo, J., Hillie, T.K., Swart, H.C., Motaung, D.E. (2020). TiO_2 nanowires for humidity-stable gas sensors for toluene and xylene. *ACS Applied Nano Materials, 4*(1), 702-716. DOI: 10.1021/acsanm.0c02963

[24] You, S.-M., El Rouby, W.M.A., Assaud, L., Doong, R.-A., Millet, P. (2021). Water Photo-Electrooxidation Using Mats of TiO_2 Nanorods, Surface Sensitized by a Metal–Organic Framework of Nickel and 1,2-Benzene Dicarboxylic Acid. *Hydrogen, 2*(1), 58-75. DOI: 10.3390/hydrogen2010004

[25] Fu, Y., Sun, D., Chen, Y., Huang, R., Ding, Z., Fu, X.,Li, Z. (2012). An amine-functionalized titanium metal-organic framework photocatalyst with visible-light-induced activity for CO_2 reduction. *Angewandte Chemie (International ed. in English), 51*(14), 3364-3367. DOI: 10.1002/anie.201108357

[26] Wang, Z., Wang, Z., Pang, Y., Wang, X.,Chen, Y. (2023). Effect of Metal Substitution on the Optical Band Gap of MIL-125-NH_2. *ChemistrySelect, 8*(44), e202301509. DOI: 10.1002/slct.202301509

[27] Makuła, P., Pacia, M.,Macyk, W. (2018). How To Correctly Determine the Band Gap Energy of Modified Semiconductor Photocatalysts Based on UV–Vis Spectra. *The Journal of Physical Chemistry Letters, 9*(23), 6814-6817. DOI: 10.1021/acs.jpclett.8b02892

[28] Fan, W.K., Tahir, M., Alias, H. (2023). Synergistic Effect of Nickel Nanoparticles Dispersed on MOF-Derived Defective Co_3O_4 In Situ Grown over TiO_2 Nanowires toward UV and Visible Light Driven Photothermal CO_2 Methanation. *ACS Applied Materials and Interfaces, 15*(47), 54353-54372. DOI: 10.1021/acsami.3c10022

[29] Jiang, H., Yu, X., Li, J., Wang, L., Wang, W., Wu, C., Tang, L., Liu, Q. (2023). Synergistic effect of Z-scheme junction and core–shell architecture over NH_2-MIL-125@Ag@AgCl ternary heterojunction for cooperative CO and H_2O_2 production. *Applied Surface Science, 639*, 158281. DOI: 10.1016/j.apsusc.2023.158281.